Bipolar Electrochemical Mechanism for the Propulsion of Catalytic Nanomotors in Hydrogen Peroxide Solutions†

Yang Wang, Rose M. Hernandez, David J. Bartlett, Jr., Julia M. Bingham, Timothy R. Kline, Ayusman Sen,* and Thomas E. Mallouk*

Department of Chemistry, The Pennsylvania State University, University Park, Pennsylvania 16802

Received June 2, 2006. In Final Form: August 9, 2006

Bimetallic nanorods are propelled in aqueous solutions by the catalytic decomposition of hydrogen peroxide to oxygen and water. Several mechanisms (interfacial tension gradients, bubble recoil, viscous Brownian ratchet, self-electrophoresis) have been proposed for the transduction of chemical to mechanical energy in this system. From Tafel plots of anodic and cathodic hydrogen peroxide reactions at various metal (Au, Pt, Rh, Ni, Ru, and Pd) ultramicroelectrodes, we determine the potential at which the anodic and cathodic reaction rates are equal for each metal. These measurements allow one to predict the direction of motion of all possible bimetallic combinations according to the bipolar electrochemical (or self-electrophoretic) mechanism. These predictions are consistent with the observed direction of motion in all cases studied, providing strong support for the mechanism. We also find that segmented nanorods with one Au end and one poly(pyrrole) end containing catalase, an enzyme that decomposes hydrogen peroxide nonelectrochemically, perform the overall catalytic reaction at a rate similar to that of nanorods containing Au and Pt segments. However, in this case there is no observed axial movement, again supporting the bipolar electrochemical propulsion mechanism for bimetallic nanorods.

Introduction

Catalyic molecular and nanoscale motors are of interest as "engines" for micrometer- and submicrometer-scale devices such as actuators, sensors, pumps, and autonomous vehicles. So far, the most efficient micro/nanoscale motors are derived from biological systems.[1] A common principle of biological nanomotors is the use of catalysis to convert the stored chemical energy of fuels, such as ATP, into mechanical energy. In contrast, most nonbiological schemes for making micro/nanoscale machines involve externally applied magnetic[2] or electrical forces.[3] Although motors of this type can be relatively efficient, the delivery of power from a macroscopic external source limits their utility.

We recently found that bimetallic Au−Pt nanorods exhibit directional movement at speeds up to 20 μm/s in aqueous H_2O_2 solutions.[4] In very similar experiments, Ozin and co-workers observed the rotation of Ni−Au nanorods.[5] These catalytic nanomotor experiments were inspired by the earlier work of Ismagilov et al., who showed that asymmetric millimeter-scale objects with Pt catalysts at one end moved autonomously at the air/H_2O_2 solution interface.[6] In that case, and in a subsequent macroscopic catalytic motor system studied by Feringa et al.,[7] the objects moved in the direction opposite to the Pt catalyst, suggesting that motion was driven by recoil from oxygen bubbles made in the reaction. Interestingly, in the bimetallic nanorod systems[4,5] and with bimetallic Au−Pt microgears,[8] the direction of motion was always the opposite (i.e., with the Pt or Ni end forward). Furthermore, the nucleation of gas bubbles was not observed on the nanorods themselves but rather on the surrounding glass surfaces, suggesting that the mechanism of energy transduction was not the same as in the macroscopic recoil-driven systems.

In designing new catalytic nanomotors and devices derived from them, it is important to understand the principles that govern their motion in the micrometer and nanometer regimes. Thus far, there is no general agreement on the mechanism of energy transduction for catalytic nanomotors. On the basis of an analysis of reaction rates, drag forces, and interfacial energies, we initially proposed an interfacial tension mechanism for the axial motion of Pt−Au nanorods in aqueous H_2O_2.[4] The basic idea of this model is that oxygen made in the reaction disrupts hydrogen bonding locally, lowering the interfacial tension between the aqueous solution and the gas-coated nanorod. Because the oxygen concentration in solution decreases toward the Au end of the rod, a net axial force develops that propels the rod in the direction of the Pt end. Fournier-Bidoz et al. suggested a bubble-driven mechanism for their nanorotors,[5] whereas Dhar et al. proposed a Brownian ratchet mechanism in which the O_2 evolved at one end of the rod locally decreases the viscosity, allowing thermal motion to drive it that way preferentially.[9] We also considered an electrokinetic mechanism[10] in which the disproportionation of H_2O_2 occurs asymmetrically at the two metal surfaces:

$$\text{anode: } H_2O_2(aq) \rightarrow O_2(g) + 2H^+(aq) + 2e^- \quad (1)$$

$$\text{cathode: } H_2O_2(aq) + 2H^+(aq) + 2e^- \rightarrow 2H_2O(l) \quad (2)$$

$$\text{overall: } 2H_2O_2(aq) \rightarrow O_2(g) + 2H_2O(l) \quad (3)$$

If the cathode and anode reactions occur preferentially at the Au and Pt ends of the nanorod, respectively, then protons must move

† Part of the Electrochemistry special issue.

* Corresponding authors. E-mail: tom@chem.psu.edu, asen@chem.psu.edu.

(1) Schliwa, M., Ed. *Molecular Motors*; Wiley-VCH: Weinheim, Germany, 2003.

(2) Watarai, H.; Suma, M.; Iiguni, Y. *Anal. Bioanal. Chem.* **2004**, *378*, 1693−1699.

(3) Delgado, A. V. *Interfacial Electrokinetics and Electrophroesis*; Marcel Dekker: New York, 2002.

(4) Paxton, W. F.; Kistler, K. C.; Olmeda, C. C.; Sen, A.; St. Angelo, S. K.; Cao, Y.; Mallouk, T.; Lammert, P. E.; Crespi, V. H. *J. Am. Chem. Soc.* **2004**, *126*, 13424−13431.

(5) Fournier-Bidoz, S.; Arsenault, A. C.; Manners, I.; Ozin, G. A. *Chem. Commun.* **2005**, 441−443.

(6) Ismagilov, R, F.; Schwartz, A.; Bowden, N.; Whitesides, G. M. *Angew. Chem., Int. Ed.* **2002**, *41*, 652−654.

(7) Vicario, J.; Eelkema, R.; Browne, W. R.; Meetsma, A.; La Crois, R. M.; Feringa, B. L. *Chem. Commun.* **2005**, *31*, 3936−3938.

10.1021/la0615950 CCC: $33.50
Published on Web 09/15/2006

Scheme 1. Bipolar Electrochemical Decomposition of H_2O_2 at a Pt−Au Nanorod[a]

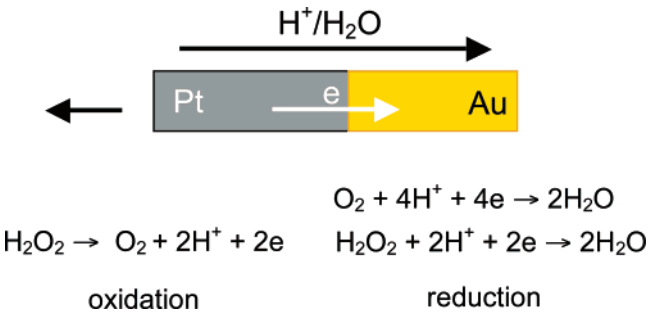

[a] In the electrokinetic mechanism, H^+ moves from the anode end to the cathode end of the rod, resulting in nanorod motion in the opposite direction. We find that whereas the electrokinetic mechanism is essentially correct the dominant cathode half reaction is actually oxygen reduction rather than H_2O_2 reduction.

from Pt to Au for charge balance (Scheme 1). In solutions of low ionic strength, the movement of protons would occur primarily in the electrical double layer at the metal−solution interface, resulting in the electroosmotic flow of water molecules from Pt to Au. By Galilean invariance, the displacement of water toward the Au end of the nanorod is equivalent to nanorod movement through the fluid in the opposite (observed) direction. We estimated that the 10−20 μm/s axial velocity of the rod could be accounted for if only a few percent of the observed oxygen evolution rate was due to the bipolar electrochemical mechanism.[10]

Two subsequent studies provided corroborating evidence for this electrokinetic mechanism. First, we found that fluid and tracer particle pumping on Ag-patterned Au surfaces occurred in H_2O_2 solutions. The direction of motion of negatively and positively charged tracer particles and the strong salt dependence of tracer particle speed were consistent with anodic and cathodic half reactions occurring on Au and Ag surfaces, respectively. Second, Mano and Heller showed that carbon fibers derivatized at two ends with "wired" redox enzymes could be propelled by the bipolar oxidation of glucose and the reduction of oxygen.[11] When an insulating layer was added to disconnect the redox enzymes from each other, no fiber movement was observed.

In the case of bimetallic nanorods, it has been difficult to determine which of the plausible mechanisms is the dominant one. At least two mechanisms (interfacial tension and self-electrophoresis) appear capable of generating axial forces in the 0.01−0.03 pN range observed, and others (diffusiophoresis, recoil, viscous Brownian ratchet) could contribute significantly under certain conditions. Direct measurements of electrocatalytic reaction rates as currents, which are possible on the 20−100 μm length scale of catalytic micropumps,[12] are difficult on the 1−2 μm scale of bimetallic nanorods. However, it is relatively straightforward to determine the potential at which the rates of reactions 1 and 2 and any other half cell reactions that are operative in the system are exactly balanced for a given catalytic metal surface. This is the mixed potential at which the net current is zero. If these mixed potential values are known for both of the metals that make up a bimetallic nanorod, then the direction of current flow, and therefore the direction of motion, can be predicted. Aside from Pt and Au, a number of relatively noble metals are catalytically active in H_2O_2 reduction and oxidation.[13]

In this article, we correlate measurements of the mixed potentials of individual catalytic metals (Pt, Pd, Ni, Au, Ru, and Rh) with the direction of motion of bimetallic nanorods in aqueous H_2O_2. The strong correlation between the predicted and observed direction of motion for combinations of these metals provides good evidence that bipolar electrochemistry is the dominant factor in generating the axial force experienced by bimetallic nanorods in H_2O_2 solutions. In this electrokinetic propulsion mechanism, internal electron flow from one end of the nanorod to the other is required for movement. In the other possible mechanisms, oxygen evolution but not current is required. Therefore, another test of the electrokinetic mechanism is to fabricate nanorods that catalyze the overall reaction (3) at a comparable rate but in an insulating nanorod. We also report here the fabrication of poly(pyrrole)−Au nanorods (Ppy−Au) in which the polymer segments contain catalase, an enzyme that performs reaction 3 without exchanging electrons with its surroundings. Although the rate of oxygen evolution is similar to that of Au−Pt nanorods of the same dimensions, these nanorods exhibit only Brownian movement in H_2O_2 solutions. This is further evidence that the axial forces generated by other mechanisms are small compared to self-electrophoretic forces.

Experimental Section

Preparation, Characterization, and Tracking of Bimetallic Nanorods. Bimetallic nanorods were made by an electroplating method as described elsewhere in detail.[14] Anodic alumina membranes (Whatman Inc., NJ, 2 cm diameter) containing cylindrical pores (nominally 200 nm in diameter) were employed as the templates for nanowire growth. The diameter of the nanowires made from this membrane was 370 nm. A thin sacrificial layer (300 nm) of Ag was evaporated onto the branched side of the membranes to serve as the working electrode contact. A Pt wire (0.3 mm diameter) was used as the counter electrode, and a 3-mm-diameter Ag/AgCl (3M NaCl) electrode (BAS) was used as the reference electrode. Deionized water (18 MΩ cm) purified by a Barnstead Nanopure system was used in all experiments. Approximately 8−10 μm of additional sacrificial Ag was electroplated into the membrane at a current density of 1.6 mA/cm^2 to fill the branched section of the pore. The electrodeposition was done in galvanostatic mode using a Pine Instruments bipotentiostat, model AFCBP1. Pt, Pd, Ni, Ag, Au, Ru, and Rh nanowire segments were grown using commercially available plating solutions obtained from Technic Inc. The Co plating condition was 7.15 g of cobalt(II) sulfate/8.54 g sodium citrate tribasic dihydrate in 100 mL of H_2O. To achieve 1-μm-long nanowire segments, Co was plated at −1.15 V for 30 min; Ag was electroplated at −1.6 mA/cm^2 for 5 min; Pt was plated at −1.6 mA/cm^2 for 40 min; Au was plated at −1.1 mA/cm^2 for 10 min; Ni was plated at −1.1 mA/cm^2 for 25 min; Pd was plated at −1.6 mA/cm^2 for 25 min; Rh was plated at −2 mA/cm^2 for 80 min; and Ru was plated at −0.63 V for 30 min. After electroplating, the nanorod-filled membranes were immersed in 5 M HNO_3 to dissolve the Ag sacrificial layer and then immersed in 5 M NaOH to dissolve the alumina membrane. Then the nanorods were centrifuged and rinsed in deionized water four to six times to remove the remaining NaOH. Metals that dissolve in HNO_3 (Pd, Ag, and Co) were plated last and were therefore protected by a layer of the other metal in the step in which the Ag sacrificial layer was dissolved. In this case, 5 M HNO_3 was added to one side of the membrane only. After removal of the template, the rods were suspended and stored in deionized water.

FE-SEM images were obtained from JEOL 6700F FE-SEM at 5 kV, 20 μA. TEM images were obtained with a JEOL 1200EXII at

(8) Catchmark, J. M.; Subramanian, S.; Sen, A. *Small* **2005**, *1*, 202−6.
(9) Dhar, P.; Fischer, Th. M.; Wang, Y.; Mallouk, T. E.; Paxton, W. F.; Sen, A. *Nano Lett.* **2006**, *6*, 66−72.
(10) Paxton, W. F.; Sen, A.; Mallouk, T. *Chem.−Eur. J.* **2005,** *11*, 6462−6470.
(11) Mano, N.; Heller, A. *J. Am. Chem. Soc.* **2005**, *127*, 11574.
(12) Paxton, W. F.; Baker, P. T.; Kline, T. R.; Wang, Y.; Sen, A.; Mallouk, T. E., submitted for publication.
(13) Schumb, W.; Satterfield, W. C.; Wentworth, R. L. *Hydrogen Peroxide*; Reinhold: New York, 1955.
(14) Martin, B. R.; Dermody D. J.; Reiss, B. D.; Fang, M.; Lyon, L. A.; Natan, M. J.; Mallouk, T. E. *Adv. Mater.* **1999**, *11*, 1021−1025.

a 80 kV accelerating voltage. The motion of the nanorods in H_2O_2 solutions was observed and recorded using an OlympusBX60M reflected-light optical microscope equipped with an Olympus U-CMAN-2 digital video camera connected to a PC. The digital camera took the video at a rate of 10 frames/s. A suspension of the nanorods in aqueous 5 wt % hydrogen peroxide was placed on a capillary microslide that had a capillary thickness of 0.2 mm and width of 2 mm (VitroCom Inc). The speed and directionality of the nanorods were measured by first capturing videos of moving nanorods and then analyzing them using a MATLAB-based motion analysis program. This program tracked the difference in position of each rod in each frame and calculated the average speed and directionality of each nanorod. Typically, for each batch of nanorods, we tracked the movement of approximately 100 nanorods for 10 s each and compared the average movement in each batch with that of other samples.

Electrochemical Potential Measurements. We used two methods to measure the mixed potential at which the anode and cathode reactions proceeded at the same rate for a given metal. The first method is to measure the potential difference of the appropriate metal ultramicroelectrode and a Ag/AgCl (3 M NaCl) reference electrode at zero current, that is, the open circuit voltage. The second method is to perform cyclic voltammetry in the potential range of oxidation and reduction of H_2O_2 and then extrapolate plots of log $|i|$ versus potential from the linear Tafel regions to the potential at which the cathodic and anodic currents are equal.[15] A BAS100B (Bioanalytical Systems, Inc) potentiostat was used for these measurements. Because of the small size (25 μm diameter) of the working ultramicroelectrodes, we used a two-electrode system (in which the 3-mm-diameter Ag/AgCl reference electrode also served as the counter electrode) instead of a three-electrode system. The solution was 5 wt % H_2O_2 without added supporting electrolyte, which is the same as the fuel solution used in observations of rod motion. The sweep rate was 10 mV/s.

Pt and Au ultramicroelectrodes were obtained from CHI Instrument Company. Both were circular disk electrodes with a 25-μm-diameter Pt or Au wire sealed in glass. For other metals, working electrodes were made by electroplating the appropriate metal onto the Au ultramicroelectrode disk. The plating solution and plating conditions were the same as those used to grow the bimetallic nanorods. Surface treatment procedures were kept consistent to ensure comparable results between electrodes as follows: Before each electrochemical experiment, we polished the ultramicroelectrode with 5 μm and then with 0.05 μm alumina on microcloth (Buehler Inc). After rinsing the polished electrodes with DI water, we sonicated the electrode to remove the alumina particles. Finally, we checked the surface of the electrode under the microscope to make sure that the surface was clean and smooth in each experiment.

Catalase-Loaded Ppy−Au Nanorods. Au−polypyrrole nanorods were grown by a similar template electrodeposition method. Au was electroplated first into the membrane, which was then soaked in pyrrole solution for 10 min prior to Ppy polymerization. Ppy nanowire segments are grown onto the Au segments from 0.0.2 M pyrrole solutions in 150 mM phosphate buffer saline (PBS) at pH 6.8 at a constant potential of 0.9 V.[16] The composition of the PBS solution was 0.1 M KBr (99.99%, Aldrich), 0.05 M boric acid (>99.5%, Sigma), 0.05 M sodium dihydrogen phosphate (>99.0%, Sigma), and 0.1 M sodium acetate (>99.5%, Fluka), and the pH was adjusted by the addition of aqueous NaOH. The Ppy−Au nanorods were freed from the membrane in the same way as the bimetallic rods described above, except with 20% HNO_3 and 0.5 M NaOH. Catalase-modified Ppy segments were grown from solutions containing 0.2 M pyrrole and 5−10 mg/mL bovine liver catalase (VWR/CAL-BIOCHEM) in PBS (pH 7.4) at a constant potential of 0.9 V versus Ag/AgCl (3 M NaCl). O_2 evolution rates were measured by gas chromatography (Buck Scientific 910) on argon-purged 500 μL samples using a thermal conductivity detector and an ambient temperature column. Because of the instability of the encapsulated enzyme, the GC measurements were usually made within 3 days after a new batch of nanorods was made.

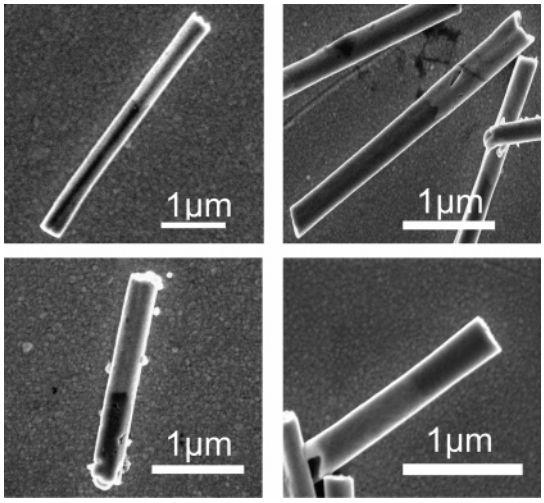

Figure 1. Field emission scanning electron micrographs of bimetallic nanorods. Clockwise from upper left: Ni−Au, Pd−Au, Pt−Rh, and Ru−Au nanorods.

Results and Discussion

Bimetallic Nanorods. Because the driving force for hydrogen peroxide disproportionation according to reaction 3 is large (1.1 V or 212 kJ/mol O_2), many different metals can catalyze the reaction.[13] However, most metals, including those that do not corrode spontaneously in water, are not oxidatively stable in H_2O_2 solutions. We therefore selected a group of metals (Pt, Pd, Ni, Au, Ru, and Rh) that gave stable and reproducible cyclic voltammetry as well as stable open circuit potentials in H_2O_2 solutions (see below). This group provides 15 unique combinations, which were fabricated as bimetallic nanorods.

The structures and aspect ratios of a few examples of these bimetallic rods are shown as SEM images in Figure 1. In the SEM images, the heavier element appears to be lighter in color because of more efficient backscattering of electrons. Typically, the nanorods have smooth sidewalls reflecting the smooth nature of the template pores. One end of the nanorod is often concave, a consequence of the fact that the growing metal nanowire wets the polar pore walls. For the purposes of this study, we prepared nanorods with an average length of 2 μm and a segment length ratio of ~1:1, which typically gives the fastest axial motion for a given pair of metals. Although not explored in great detail, our preliminarily observations show that with shorter rods the movement tends to be more random. This may be attributed to the lower catalytic surface area of the nanorods and the lower drag force that favors Brownian motion over axial propulsion. However, rods longer than about 4 μm move more slowly because of increased fluid drag and sliding friction along the glass surface of the capillary slide. Although it may be possible to optimize the relative segment lengths of 2 μm rods for motility based on the Tafel analysis of cathodic and anodic current densities, no attempt was made to do so in this study.

Of these 15 combinations, the 5 containing Ni were problematic because of their tendency to aggregate through magnetic interactions. Using very dilute Au−Ni nanorod suspensions, we confirmed catalytic axial movement with Ni ends forward, as reported earlier by Fournier-Bidoz et al.[5] Two other bimetallic combinations, Rh−Ru and Pd−Ru, resulted in either highly porous rod surfaces or weakly joined rods that disintegrated at

(15) Bard, A. J.; Faulkner, L. R. *Electrochemical Methods: Fundamentals and Applications*, 2nd ed.; John Wiley & Sons: New York, 2001.

(16) Hernandez, R. M.; Richter, L.; Semancik, S.; Stranick, S.; Mallouk, T. E. *Chem. Mater.* **2004**, *16*, 3431−3438.

Table 1. Tracking Data for Bimetallic Nanorods in 5 wt % Aqueous H_2O_2 Solution[a]

bimetallic nanorod	speed (μm/s)	directionality	leading end (observed)	leading end (predicted)
Rh−Au	23.8 ± 2.9	0.73 ± 0.15	Rh	Rh
Pt−Au	20.0 ± 3.8	0.84 ± 0.04	Pt	Pt
Pd−Au	15.3 ± 2.0	0.92 ± 0.05	Pd	Pd
Pt−Ru	30.2 ± 4.0	0.65 ± 0.11	Pt	Pt
Au−Ru	24.0 ± 2.0	0.90 ± 0.05	Au	Au
Rh−Pt	17.0 ± 3.0	0.79 ± 0.13	Rh	Rh
Rh−Pd	16.2 ± 1.8	0.84 ± 0.14	Rh	Rh
Pt−Pd	13.6 ± 2.3	0.63 ± 0.10	Pt[b]	Pt
Ni−Au	4.75 ± 1.1	0.33 ± 0.12	Ni	Ni
Ag−Au	6.20 ± 1.2	0.20 ± 0.12	Ag	
Au−Co	7.10 ± 1.4	0.30 ± 0.15	Au	

[a] Combinations that were not measured: Rh−Ru, Pd−Ru, Ni−Pt, Ni−Pd, Ni−Rh, and Ni−Ru. [b] Determination based on the three-segment rods: Pt(1.5 μm)−Au(0.5 μm)−Pd(1 μm) and Pt(1 μm)−Au(0.5 μm)−Pd(1.5 μm).

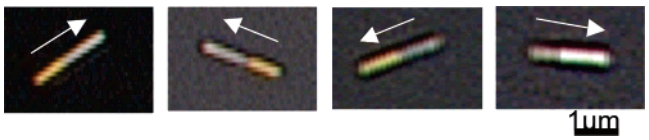

Figure 2. Optical images of (left to right) NiAu, AuPd, AuRu, and RhPt nanorods. The direction of motion is indicated by the arrow in each case.

the bimetal interface during removal from the template. This left nine combinations for which the direction of motion and axial velocity could be determined. We additionally examined several combinations that contained metals (Co and Ag) that are unstable in H_2O_2 solutions. Although the direction of motion could be observed in these cases, the mixed potential values changed substantially with time of exposure to the solution.

The catalyzed movement of bimetallic nanorods in 5 wt % (approximately 1.7 M) aqueous H_2O_2 solutions was observed by optical microscopy. The average speed of each type of nanorod and the average directionality, which is defined as the cosine of the angle between the rod axis and the direction that it moves in a given time step,[4] are summarized in Table 1. With the exception of Pt−Pd, all metal combinations that we report here have sufficient optical contrast in white light that we can differentiate the two segments and therefore determine the direction of motion. Pt−Pd was the one combination in which the color and contrast of the two metals were too similar for an unambiguous determination of the direction of motion. In this case, to determine the direction of movement, we also made three-segment rods with a longer Pt end and repeated the experiment. The results with Pt(1.5 μm)−Au(0.5 μm)−Pd(1 μm) and Pt(1 μm)−Au(0.5 μm)−Pd(1.5 μm) rods support the prediction (see below) that two-segment Pt−Pd rods should move with the Pt end forward. Representative optical images of the bimetallic rods are shown in Figure 2.

Although both translational and rotational movement of rods were observed with all metal pairs, as reported elsewhere,[5] rotational movement was more frequently observed with rods that were either (1) very short, (2) had somewhat obvious asymmetry with respect to the shape of the rod, or (3) were clearly held down to the surface of the capillary slide at one end.

Tafel Plots and Mixed Potential Measurements. Figure 3 shows a comparison of Tafel plots for Pt and Ru ultramicroelectrodes. Similar results were obtained with the other noble metals studied (Rh, Ni, Pd, and Au). In each case, there was an approximately linear Tafel regime in the range of log $|i| = -8.0$ to -7.0. The mass-transfer-limited current at a 25-μm-diameter

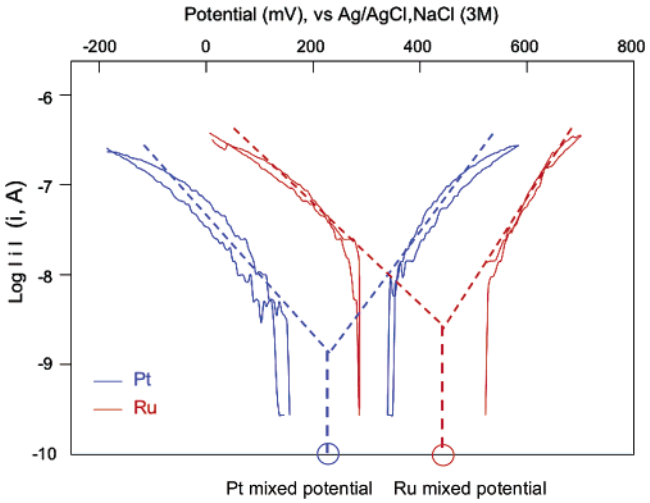

Figure 3. Tafel plots for Pt and Ru ultramicroelectrodes in 5 wt % H_2O_2 solutions. The intersections of red and blue dotted lines represent mixed potential values for Ru and Pt, respectively, as indicated by circles on the potential axis. The potential of a bimetallic nanorod in this medium is given approximately by the intersection of the cathodic red and anodic blue dotted lines.

disk is given by eq 4, where $n = 2$ for reaction 1. Taking $D \approx 1 \times 10^{-5}$ cm^2/s, $C = 1.7 \times 10^{-3}$ mol/cm^3, and $r = 1.3 \times 10^{-3}$ cm, we obtain $i_l \approx 2 \times 10^{-5}$ A, which is much larger than the currents

$$i_l = 4nFDCr \tag{4}$$

measured. The curvature in the plots beyond $|i| \approx 10^{-7}$ A is therefore most likely due to uncompensated solution resistance in the absence of supporting electrolyte. The solution resistivity was 2×10^5 Ω cm, consistent with this hypothesis. By extrapolating the linear Tafel regions of the anodic and cathodic branches to their point of intersection, a mixed potential was obtained for each metal, as shown in Figure 3. Very similar values were obtained by simply measuring the open circuit voltage between each ultramicroelectrode and the Ag/AgCl reference electrode. In either cas,e we find a difference of approximately 170 mV between the mixed potentials of Pt and Ru in 5% H_2O_2. Because Ru is positive with respect to Pt, we expect Ru to act as the cathode in the bipolar electrochemical reaction. This means that electrons, protons, and water molecules (by electroosmotic drag) should move from Pt to Ru and therefore the rod should move with its Pt end forward. We would also expect relatively fast motion because of the large potential difference. This is in fact observed, as Pt−Ru rods move with their Pt end forward at an average speed of ~30 μm/s.

Table 2 shows that the sequence of the mixed potentials is Rh < Pt < Ni < Pd < Au < Ru. There is generally good agreement with values obtained from Tafel analysis and from direct measurement of open circuit potentials. The experimental results of the direction of motion for the nine measured combinations of Rh, Pt, Pd, Au, and Ru agree well with predictions based on the mixed potential data (Table 1). Ag and Co do not have stable mixed potentials because of their instability in H_2O_2 solutions. Their Tafel plots showed significant hysteresis, and open circuit potentials measured with these metals varied with time. Because the range of measured mixed potentials was very large for Ag and Co, we cannot draw any definitive conclusions from their observed direction of movement in bimetallic nanorods.

The mixed potentials in Table 2 range from +0.20 to +0.41 V versus Ag/AgCl (3 M NaCl). Considering that the standard

Table 2. Mixed Potential Data for Electroplated Metals in 5 wt % Aqueous H_2O_2

	Rh	Pt	Ni	Pd	Au	Ru	Ag	Co
mixed potential from Tafel plot	200	232	253	244	274	405		
(mV, vs Ag/AgCl)	+/−8	+/−5	+/−4	+/−10	+/−6	+/−14		
mixed potential from open circuit voltage	206	250	258	263	280	390	202−350	211−264
(mV, vs Ag/AgCl)	+/−6	+/−13	+/−9	+/−9	+/−6	+/−27		

potentials of reactions 1 and 2 are 0.15 and 1.21 V versus Ag/AgCl (3 M NaCl), respectively, at pH 5.6, the mixed potentials in Table 2 are much closer to the potential of the peroxide oxidation reaction than to that of the peroxide reduction reaction. This suggests that at least one other cathodic reaction is involved in the overall electrochemistry. A number of studies on the electrochemistry of H_2O_2 at various metals have shown that in addition to reaction 2 the four-electron reduction of O_2 to H_2O (reaction) occurs:[17−21]

$$O_2(g) + 4H^+(aq) + 4e^- \rightarrow 2H_2O(l) \quad (5)$$

The standard potential of reaction 4 is 0.68V versus Ag/AgCl (3 M NaCl), which is much closer to the measured mixed potential than that of reaction 2. We can thus write the predominant pair of half-cell reactions driving the self-electrophoretic movement of the nanorods as

$$\text{anode: } 2H_2O_2(aq) \rightarrow 2O_2(g) + 4H^+(aq) + 4e^- \quad (6)$$

$$\text{cathode: } O_2(g) + 4H^+(aq) + 4e^- \rightarrow 2H_2O(l) \quad (5)$$

$$\text{overall: } 2H_2O_2(aq) \rightarrow O_2(g) + 2H_2O(l) \quad (3)$$

where eq 6 is simply anode reaction 1 multiplied by 2. As expected from this analysis, metals that have the lowest overpotential for reaction 4, namely, Pt and Rh, have the most negative mixed potentials in Table 2 and tend to make the fastest-moving bimetallic combinations.

Figure 4 shows the trend in average rod speed versus mixed potential difference obtained by combining the data from Tables 1 and 2. There is a clear trend toward faster movement with larger difference in mixed potentials. Although effects such as local pH and the surface areas of the two segments are factors in determining the potential and current density of a bimetallic nanorod in hydrogen peroxide solution, information on trends may be obtained from Tafel plots such as those shown in Figure 3. The intersection of the cathodic and anodic branches of $i-V$ curves of the more positive and more negative metals, respectively, indicates the potential and current that would result if ultramicroelectrodes of the two metals were connected electrically. Referring to Figure 3, this is the central intersection point of the blue and red dotted lines. This intersection occurs at higher current when the difference in mixed potentials of the two metals is larger, consistent with the trend observed in Figure 4.

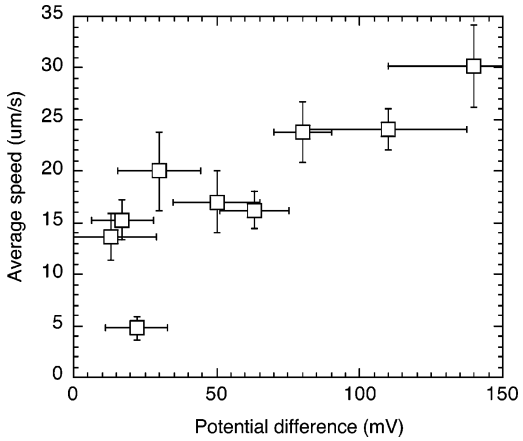

Figure 4. Plot of average rod speed vs mixed potential difference for bimetallic nanorods in 5 wt % H_2O_2 solution.

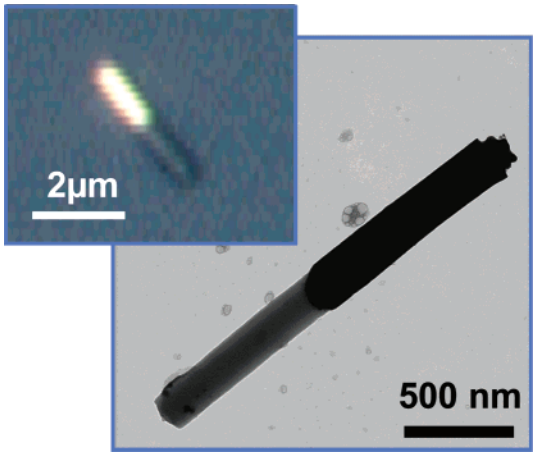

Figure 5. Optical micrograph of a catalase−Ppy−Au nanorod (left) and TEM image of a Ppy−Au nanorod (right).

Catalase-Loaded Au−Poly(pyrrole) Nanorods. Figure 5 shows an optical micrograph of the catalase−Ppy−Au nanorods and a TEM image of the Au−Ppy nanorods with 1 μm segments of both gold and Ppy. The purpose of this structure is to reproduce the geometric features that determine the drag forces, concentration profiles, and so forth of bimetallic nanorods. The nonelectroactive enzyme catalase was chosen to impart high catalytic activity for overall reaction 3 to the polymer segment without allowing a direct electrochemical connection between the active site of the enzyme and the gold segment of the nanorod.

Catalase has one of the highest turnover rates of all known enzymes: 1 molecule of catalase can decompose approximately 10^5 molecules of H_2O_2 per second.[22] Bovine liver catalase was immobilized into the Ppy segments of the nanorods by physical entrapment during polymer electrodeposition, as demonstrated earlier for avidin and streptavidin.[16] Although the amount of catalase incorporated is not known quantitatively, we found that

(17) Bianchi, G.; Mazza, F.; Mussini, T. *Electrochim. Acta* **1966**, *11*, 1509−1523.
(18) (a) Honda, M.; Kodera, T.; Kita, H. *Electrochim. Acta* **1986**, *31*, 377−383. (b) Honda, M.; Kodera, T.; Kita, H. *Electrochim. Acta* **1983**, *28*, 727−733. (c) Flatgen, G.; Wasle, S.; Lubke, M.; Eickes, C.; Radhakrishnan, G.; Doblhofer, K.; Ertl, G. *Electrochim. Acta* **1999**, *44*, 4499−4506.
(19) Hall, S. B.; Nairn, J. J.; Khudaish, E. A. *Phys. Chem. Chem. Phys.* **2001**, *3*, 4566−4572.
(20) Prabhu, V. G.; Zarapkar, L. R.; Dhaneshwar, R. G. *Electrochim. Acta* **1981**, *26*, 725−729.
(21) Janasek, D.; Vastarella, W.; Spohn, U.; Teuscher, N.; Heilmann, A. *Anal. Bioanal. Chem.* **2002**, *374*, 1267−1273.
(22) (a) Aydemir, T.; Kuru, K. *Turk. J. Chem.* **2003**, *27*, 85−98. (b) Betancor, L.; Hidalgo, A.; Fernandez-Lorente, G.; Mateo, C.; Fernandez-LaFuente, R.; Guisan, J. M. *Biotechnol. Prog.* **2003**, *19*, 763−767.

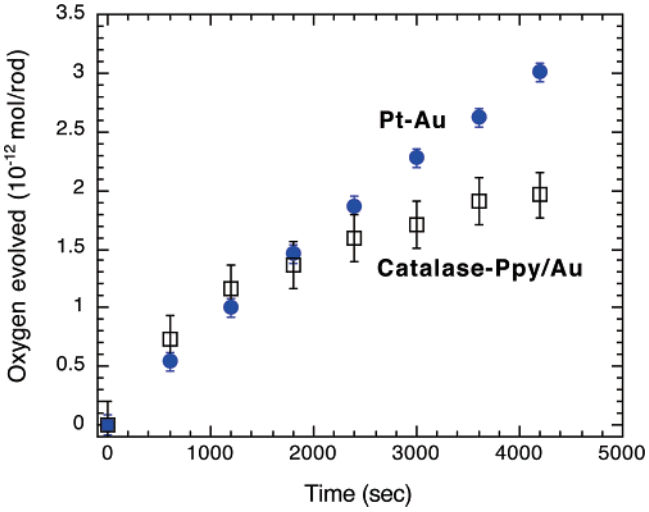

Figure 6. Oxygen evolved as a function of time for stirred suspensions of Au−Pt nanorods and catalase−Ppy−Au nanorods in 5 wt % aqueous H_2O_2 solution.

the rate of oxygen evolution from the most-active batches of these nanorods was comparable to that observed with Pt−Au nanowires. Figure 6 shows a plot of oxygen evolved versus time for Au−Pt nanorods and catalase−Ppy−Au rods in unbuffered 5% H_2O_2 solution. The oxygen evolution rate at Au−Pt is 7.3 $\times$ 10^{-16} mol(O_2)/s per nanorod and is relatively constant over 1 h. The catalase−Ppy−Au nanorods initially evolve oxygen at a slightly higher rate than the Au−Pt nanorods, but the reaction rate decreases over the course of 30−60 min, presumably due to enzyme denaturation in this medium. Because all of our observations of the movement of the nanorods were made within the first 20 min, the Au−Pt and catalase−Ppy−Au nanorods effectively have very similar oxygen evolution rates. Nevertheless, only Brownian motion was found with catalase-loaded Ppy−Au nanorods in aqueous H_2O_2.

Conclusions

Taken together, these observations provide very strong support for a bipolar electrochemical propulsion mechanism in the case of bimetallic nanorods. This mechanism faithfully predicts the direction of motion for all electrochemically stable combinations of metals that were measured. The mixed potentials measured for individual catalytic metals further suggest that the dominant cathode reaction is the four-electron reduction of oxygen to water and not hydrogen peroxide reduction as we had previously postulated. Although other factors (such as surface roughness, metal zeta potential, and exchange current densities of specific metals) contribute to the magnitude of the axial force, there is nevetheless a correlation between the mixed potential difference and the speed of the bimetallic nanorods. The negative result obtained with catalase-loaded Ppy−Au nanorods shows that the nonelectrochemical decomposition of H_2O_2 (which should generate sufficient force to drive movement in the bubble recoil, viscous Brownian ratchet, and interfacial tension mechanisms) does not contribute significantly to propulsion.

With the knowledge that the same electrokinetic mechanism drives both the catalytic nanomotors and micropumps that we have studied to date, it may be possible to design better or more versatile motor systems. For example, nanomotors and pumps that are more energy efficient might be developed by selecting redox partners that have high electrochemical rates (i.e., large differences in mixed potentials) but low individual catalytic turnover rates for the decomposition of H_2O_2 or similar fuels. Other combinations of oxidizing and reducing agents should be possible, and the glucose−oxygen system studied by Mano and Heller already provides one very interesting example of this.[11] Finally, it is important to note that nonelectrochemical catalytic nanomotors, especially those that utilize hydrolysis or polymerization reactions, are ubiquitous in biology. These biomotors provide an existence proof that argues for the future design of synthetic nanomotors based on similar principles.

Acknowledgment. Financial support for this project was provided by the Penn State Center for Nanoscale Science (NSF-MRSEC, DMR-021362). D.J.B. was supported by a Teas Summer Undergraduate Scholarship from the Penn State Department of Chemistry. We also thank an anonymous reviewer for helpful suggestions on the interpretation of the mixed potential data.

LA0615950